Available online at www.sciencedirect.com
SCIENCE DIRECT®
Journal of Sound and Vibration 292 (2006) 341–371
JOURNAL OF SOUND AND VIBRATION
www.elsevier.com/locate/jsvi

Linear thermoelastic buckling and free vibration behavior of functionally graded truncated conical shells

Rajesh K. Bhangale, N. Ganesan*, Chandramouli Padmanabhan*

Machine Design Section, Department of Mechanical Engineering, Indian Institute of Technology Madras, Chennai 600 036, India

Received 2 December 2004; received in revised form 3 June 2005; accepted 29 July 2005
Available online 3 October 2005

Abstract

In recent years, structures made up of functionally graded materials (FGMs) have received considerable attention for use in high-temperature applications. In this article, a finite element formulation based on First-Order Shear Deformation Theory (FSDT) is used to study the thermal buckling and vibration behavior of truncated FGM conical shells in a high-temperature environment. A Fourier series expansion for the displacement variable in the circumferential direction is used to model the FGM conical shell. The material properties of the truncated FGM conical shells are functionally graded in the thickness direction according to a volume fraction power law distribution. Temperature-dependent material properties are considered to carry out a linear thermal buckling and free vibration analysis. The conical shell is assumed to be clamped–clamped and has a high temperature specified on the inner surface while the outer surface is at ambient temperature. The one-dimensional heat conduction equation is used across the thickness of the conical shell to determine the temperature distribution and thereby the material properties. In addition, the influence of initial stresses on the frequency behavior of FGM shells has also been investigated. Numerical studies involving the understanding of the role of power law index, r/h ratios, and semi-vertex angle on the thermal buckling temperature as well as on vibration have been carried out.

*Corresponding authors.
E-mail addresses: rajesh_phd@iitm.ac.in (R.K. Bhangale), nganesan@iitm.ac.in (N. Ganesan), mouli@iitm.ac.in (C. Padmanabhan).

0022-460X/$ - see front matter © 2005 Elsevier Ltd. All rights reserved.
doi:10.1016/j.jsv.2005.07.039

1. Introduction

In recent years, functionally graded materials (FGMs) have been developed due to their excellent mechanical and thermal properties. These materials are high performing and heat resistant, capable of withstanding ultrahigh temperatures and extremely large gradients present in spacecraft and nuclear applications. FGMs are microscopically inhomogeneous composite materials. The concept of FGM was first proposed in 1984 by a group of materials scientists, in Sendai, Japan, as novel materials with thermal barrier or heat-shielding properties. Research activities have been accelerated within Japan and worldwide in the recent past [1–3]. Typically, these materials are usually made from a mixture of metals and ceramic through a powder metallurgy process. The advantage of using these materials is that they are able to withstand high-temperature gradient environments while maintaining their structural integrity. For example, the insulating tile for a re-entry space vehicle can be designed such that the outside is a refractory (ceramic) material, and the inside a load-carrying structure made of a strong and tough metal [4]. It possesses properties that vary gradually and continuously with respect to the spatial coordinates in order to achieve a required function. The composition is varied from a ceramic-rich surface to a metal-rich surface with a desired variation of the volume fraction of the two materials in between the two surfaces [5]. Initially, FGMs were designed as thermal barrier materials for aerospace application and fusion reactors. Later on, FGMs were developed for military, automotive, biomedical application, semi-conductor industry and general structural element in high thermal environments.

A truncated conical shell is one of the main components of the propulsion system structure in rockets. Truncated conical shells are also used to contain liquids. Instability of truncated conical shells under thermal loading was studied by Lu and Chang [6,7]. They presented the parameter study on truncated conical shells for two cases of temperature distribution: temperature gradient along the generator of the cone and temperature changes circumferentially and meridionally. Evaluation of the critical temperature and its relation to geometric parameters were discussed. It was found that axial compression or bending was the primary cause for thermal buckling. Dumir et al. [8] have analyzed truncated conical caps for static and dynamic buckling loads using first-order shear deformation and classical lamination theory. Stern [9] derived the differential equations for the problem of thermal stresses in conical shells subjected to axially symmetric temperature distribution. Huth [10] derived the equations for the computation of thermal stresses in conical shells (applicable to conical missile tips flying at zero angle of attack), which takes into account the aerodynamic pressure and thermal gradient. Material properties used for the analysis, however, were independent of temperature. Bushnell and Smith [11] have carried out experimental and computer software BOSOR to analyze thermal buckling of conical shells. Tani [12] studied the effect of axisymmetric initial deflections on the thermal buckling of shallow, truncated conical shells under uniform heating. Lakis et al. [13] have carried out dynamic analysis of anisotropic fluid-filled conical shells. Likewise, Jianping and Harik [14] presented thermal stress analysis on the axisymmetric conical shells of tapered thickness subjected to aerodynamic pressure and thermal gradient. An iterative finite difference technique was used to solve the governing partial differential equations derived from thin shell theory. Temperature was assumed to vary along the meridian and thickness of the shell and temperature-dependent material properties were used

in the analysis. Wu and Chiu [15] formulated asymptotic equations for laminated circular conical shells subjected to static and periodic thermal loads, and using the differential quadrature method and Bolotin's method, the boundary frequencies of dynamic instability regions were determined.

In recent years, studies on FGM structures in thermal environments are an attractive emerging area in the research community. Reddy and Chin [16] have developed coupled as well as uncoupled thermoelastic finite element formulation for analyzing the thermomechanical behavior of functionally graded cylinders and plates subjected to abrupt thermal loading. Parametric study involved the variation of the volume fraction index in order to evaluate the temperature field and stress field. Numerical results were illustrated by simulating the start up period of the cylindrical pipes carrying hot gases typical of a situation in advanced gas turbine plants. Liew et al. [17] have derived an analytical model to carry out studies on functionally graded hollow cylinders subjected to arbitrary steady state and transient temperature field. Steady-state temperature distribution, thermal stresses and thermal displacements in a functionally graded cylinder are illustrated. A comprehensive review on the literature related to thermally induced bending, buckling and postbuckling behavior and vibration of plates at elevated temperature and rapid heating can be found in the review article by Tauchert [18]. Praveen et al. [19] have developed a thermoelastic finite element model to study the response of a functionally graded cylinder subjected to rapid heating. The analysis takes into account the material properties variations with temperature. Sofiyev [20] studied the stability of functionally graded truncated conical shells subjected to aperiodic impulsive loading. Recently, Bhangale and Ganesan [21] developed a decoupled thermoelastic finite element analysis for thermal buckling behavior of a functionally graded beam.

However, studies on thermal buckling analyses of FGM shells are rare in the literature. Shahsiah and Eslami [22] using Sanders nonlinear strain–displacement relation and first-order shell theory derived the equilibrium and stability equations for a functionally graded cylindrical shell. The authors [23] developed coupled fluid structure formulation for free vibration and buckling analysis of functionally graded cylindrical shells conveying hot liquid sodium by finite element method. Thermal buckling analysis of FGM shells was carried out for a thermal loading arising from a uniform temperature rise and a radial temperature difference. Recently, Kadoli [24] has carried out thermal buckling analysis for FGM cylindrical shells using the finite element method. Most recently, Bhangale and Ganesan [25] carried out thermal buckling analysis of FGM hemispherical shells with a cut-out at the apex by the finite element method.

Thermal buckling studies of conical shells, which take into account temperature-dependent material properties, are rarely reported in the literature. To the best of the authors' knowledge, there are no studies in the open literature on thermal buckling and vibration behavior of truncated FGM conical shells by the finite element method. In the present study, an attempt has been made to do the same. The present studies consider temperature distribution, given the temperature boundary conditions, based on the temperature-dependent material property and subsequently considering the thermal loading to compute initial stresses and hence solving the static thermal stability problem by using semi-analytical finite element. The iterative procedure has been adopted for computing material properties dependent on temperature distribution for the evaluation of thermal buckling temperature.

2. Analytical model of FGM material properties

FGMs are typically made from a mixture of ceramic and metal or a combination of different metals. The present study considers FGMs composed of metal and ceramic. The grading is accounted for only across the thickness of the shell. The present approach adopts the smooth and continuous variation of the volume fraction of either ceramic or metal based on the power law index. The present work assumes no pores and makes use of only the smooth and continuous variation of the volume fraction of the ceramic or metal based on the power law index. To start with, a simple power law-type definition for the volume fraction of the metal across the radial direction of the shell is assumed. This is defined as

$$V_f = \left(\frac{2z+h}{2h}\right)^n. \tag{1}$$

Based on the above definition, it follows that the inner surface of the conical shell will be ceramic rich. The above definition and other definitions to follow are available in Ref. [16]. This simple rule of mixture model does provide a reasonably accurate prediction of the mechanical as well as thermal properties of these inhomogeneous materials. The sum total volume of the constituent materials, ceramic (c) and metal (f), should be

$$V_c + V_f = 1. \tag{2}$$

Based on the volume fraction definition and law of mixtures, the effective material property definition follows:

$$(\mathrm{MP})_{\mathrm{eff}} = (\mathrm{MP})_{\mathrm{ot}} V_f + (\mathrm{MP})_{\mathrm{in}} V_c. \tag{3}$$

'MP' is a general notation for material property. Making use of Eqs. (1)–(3), the following effective mechanical and thermal properties definitions can be written:

$$E_{\mathrm{eff}} = (E_{\mathrm{ot}} - E_{\mathrm{in}})\left(\frac{2z+h}{2h}\right)^n + E_{\mathrm{in}}, \tag{4a}$$

$$v_{\mathrm{eff}} = (v_{\mathrm{ot}} - v_{\mathrm{in}})\left(\frac{2z+h}{2h}\right)^n + v_{\mathrm{in}}, \tag{4b}$$

$$\rho_{\mathrm{eff}} = (\rho_{\mathrm{ot}} - \rho_{\mathrm{in}})\left(\frac{2z+h}{2h}\right)^n + \rho_{\mathrm{in}}, \tag{4c}$$

$$k_{\mathrm{eff}} = (k_{\mathrm{ot}} - k_{\mathrm{in}})\left(\frac{2z+h}{2h}\right)^n + k_{\mathrm{in}}, \tag{4d}$$

$$\alpha_{\mathrm{eff}} = (\alpha_{\mathrm{ot}} - \alpha_{\mathrm{in}})\left(\frac{2z+h}{2h}\right)^n + \alpha_{\mathrm{in}}. \tag{4e}$$

In the above Eqs. (4a)–(4e), the subscript 'ot' stands for outer surface and 'in' stands for inner surface of the conical shell. In addition to the variation of material properties in the radial direction based on the power law index, it is also possible to consider the above definitions of material properties as a function of temperature. The temperature coefficients metals, such as

stainless steel SUS304, Nickel, Ti–6Al–4V, and ceramics, such as zirconia (ZrO_2), alumina (Al_2O_3) and silicon nitride (Si_3N_4), have been taken from Reddy and Chin [16]. Based on the temperature coefficients, the temperature-dependent material properties are evaluated as follows:

$$P = P_0(P_{-1}\hat{T}^{-1} + 1 + P_1\hat{T} + P_2\hat{T}^2 + P_3\hat{T}^3), \tag{5}$$

where $\hat{T}$ represents absolute temperature in Kelvin and P_{-1}, P_1, P_2 and P_3 are coefficients of temperature $\hat{T}^{-1}$, $\hat{T}$, $\hat{T}^2$ and $\hat{T}^3$, respectively, obtained after factoring out P_0 from a cubic curve fit of the property and are unique to a particular material. Thus, the effective material properties of Eq. (3) can truly be represented as a function of thickness as well as temperature:

$$\mathrm{MP}_{\mathrm{eff}}(\hat{T}, z) = \mathrm{MP}_f(\hat{T})V_f(z) + \mathrm{MP}_c(\hat{T})V_c(z). \tag{6}$$

3. Finite element formulation

A finite element formulation based on first-order shear deformation theory (FSDT) is used to study the thermal buckling and vibration behavior.

A Fourier series expansion for the displacement variable in the circumferential direction is used to model the FGM conical shell. The (s, θ, z) coordinate system for conical shells and finite element discretization shown in Fig. 2 is as follows:

$$u(s, \theta, z, t) = u_0(s, \theta, t) + z\psi_s(s, \theta, t), \tag{7}$$

$$v(s, \theta, z, t) = v_0(s, \theta, t) + z\psi_\theta(s, \theta, t), \tag{8}$$

$$w(s, \theta, z, t) = w_0(s, \theta, t), \tag{9}$$

where u_0, v_0 and w_0 are displacements of mid-surface along the s, θ and z direction and ψ_s and ψ_θ are rotations of the normal to the mid-surface along s and θ axis, respectively. In the semi-analytical method, the generalized displacement field is assumed to depend on the circumferential direction and is expressed using Fourier series as follows:

$$\begin{Bmatrix} u_0 \\ v_0 \\ w_0 \\ \psi_s \\ \psi_\theta \end{Bmatrix} = \sum_{m=0}^{\infty} \begin{bmatrix} \cos m\theta & 0 & 0 & 0 & 0 \\ 0 & \sin m\theta & 0 & 0 & 0 \\ 0 & 0 & \cos m\theta & 0 & 0 \\ 0 & 0 & 0 & \cos m\theta & 0 \\ 0 & 0 & 0 & 0 & \sin m\theta \end{bmatrix} \begin{Bmatrix} u_{0\mathrm{m}} \\ v_{0\mathrm{m}} \\ w_{0\mathrm{m}} \\ \psi_{s\mathrm{m}} \\ \psi_{\theta\mathrm{m}} \end{Bmatrix}, \tag{10}$$

where 'm' indicates the harmonic number (or circumferential mode number). The kinematic relation for a doubly curved shell of revolution in the (s, θ, z) coordinate based on FSDT is

as follows:

$$\begin{aligned}
\varepsilon_{ss} &= \partial u/\partial s,\\
\varepsilon_{\theta\theta} &= (1/r)(\partial v/\partial\theta + u\sin\beta_{sv} + w\cos\beta_{sv}),\\
\gamma_{\theta z} &= (1/r)\left(\partial w/\partial\theta - v\cos\beta_{sv}\right) + \partial v/\partial z,\\
\gamma_{s\theta} &= (1/r)\left(\partial u/\partial\theta - v\sin\beta_{sv}\right) + \partial v/\partial s,\\
\gamma_{sz} &= \partial w/\partial s + \partial u/\partial z.
\end{aligned} \tag{11}$$

In the above equations, β_{sv} represents the semi-vertex angle of the cone as shown in Fig. 1. The total strains are denoted as ε_{ss}, $\varepsilon_{\theta\theta}$, $\gamma_{\theta z}$, γ_{sz} and $\gamma_{s\theta}$, which comprise the normal strains and the

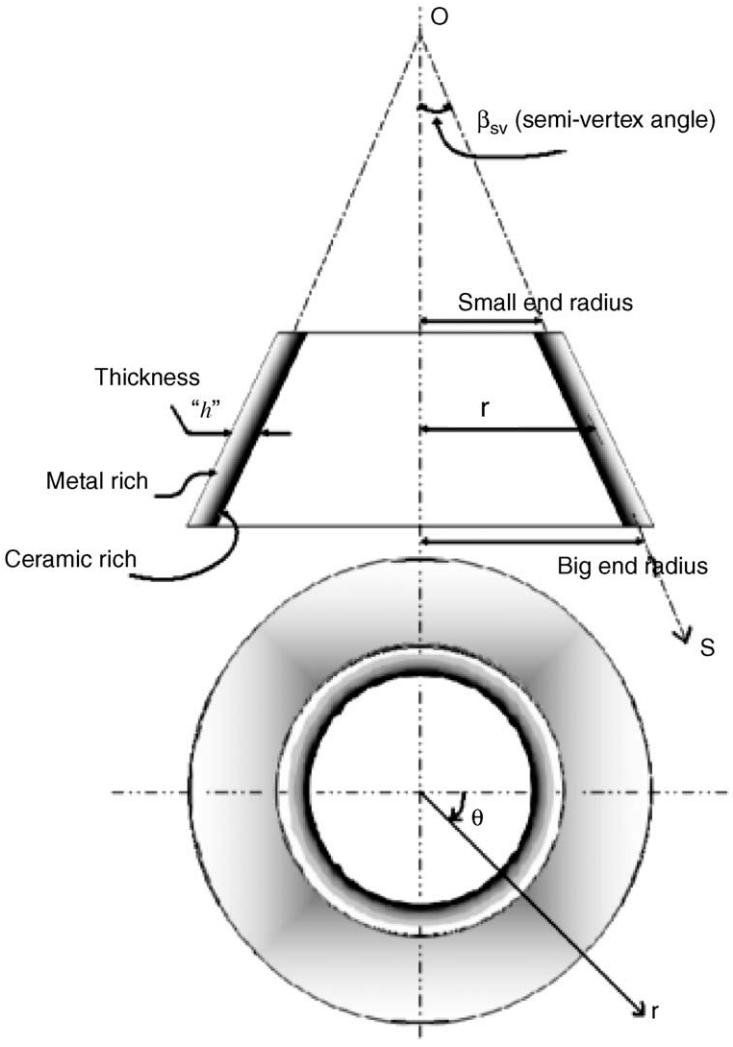

Fig. 1. Schematic configuration of the FGM truncated conical shell analyzed in the present study with a semi-vertex angle at the apex.

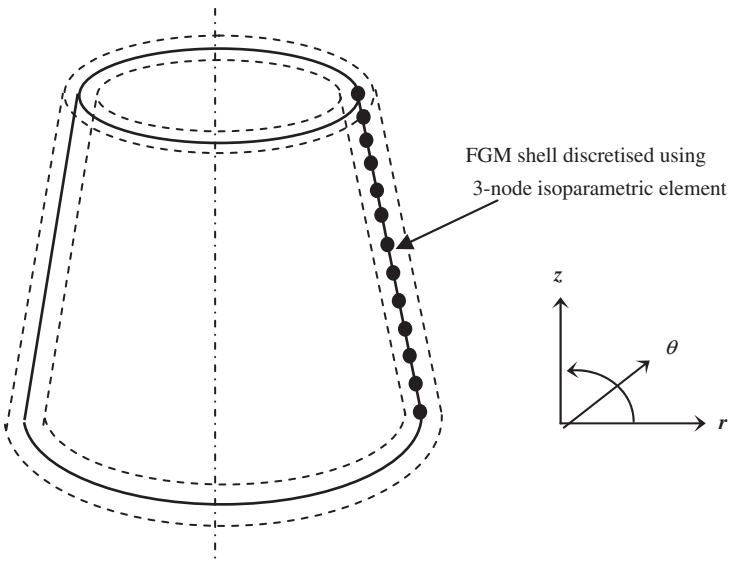

Fig. 2. Schematics of the discrimination of the FGM conical shell using three-noded quadratic line elements.

shear strains. Strain–displacement relations are used to formulate the stiffness and mass matrix. A three-noded isoparametric line element is used along the s coordinate to generate the finite element mesh for the conical shell (see Fig. 2). Each node has five degrees of freedom (DOFs). The displacements parameters associated with the element are

$$\mathbf{d}_e^{\mathrm{T}} = \{u_1, v_1, w_1, \psi_{s1}, \psi_{\theta 1}, u_2, v_2, w_2, \psi_{s2}, \psi_{\theta 2}, u_3, v_3, w_3, \psi_{s3}, \psi_{\theta 3}\}. \tag{12}$$

The shape functions N_i in terms of the isoparametric axial coordinate $\beta = \bar{s}/l$ (where $\bar{s}$ denotes the distance of a point on the element along the s-coordinate and l is the length of the element) are given by

$$N_1 = \frac{(\beta^2 - \beta)}{2}, \quad N_2 = (1 - \beta^2) \text{ and } N_3 = \frac{(\beta^2 + \beta)}{2}. \tag{13}$$

The displacement vector within the element is interpolated from the nodal DOF vector $\mathbf{d}_e$

$$\mathbf{u} = \mathbf{N}\mathbf{d}_e, \tag{14}$$

where $\mathbf{u}^{\mathrm{T}} = (u\ v\ w)$. Strains are obtained from displacements by differentiation. Thus, $\varepsilon = [\partial]\mathbf{u}$ yields $\varepsilon = \mathbf{B}^*\mathbf{d}_e$, where $\mathbf{B}^* = [\partial]\mathbf{N}$ and $[\partial]$ is the differential operator matrix given by the strain–displacement relations. The semi-analytical finite element formulation for the stiffness matrix, mass matrix, evaluation of the thermal load vector, initial stress resultants and moment resultants and finally the initial stiffness matrix will be similar to the one discussed in Ref. [26].

4. Reduced stiffness matrix for functionally graded conical shells

The difference between the structural analyses of isotropic materials, laminated composite materials and the FGMs lies in computing the material constitutive matrix, which contains the

extensional, coupling and bending terms. In case of laminated composites, the reduced integrated stiffnesses are evaluated independently for each lamina using the material properties in the material coordinates and performing coordinate transformation to the structural coordinates and summing the respective constants for all the plies or layers. In the present study, a similar approach is also adopted for the case of FGM with the difference being that one need not carry out any coordinate transformation. Considering the composition of the constituent material to vary in the thickness direction smoothly and continuously, it is possible to consider the FGM to be composed of a number of layers of very small thickness and apply the same procedure of computing the reduced stiffness coefficient, as is followed for laminated composites. The stress–strain relation for a generally isotropic material including the temperature effects is given by

$$\begin{Bmatrix} \sigma_{ss} \\ \sigma_{\theta\theta} \\ \tau_{s\theta} \\ \tau_{sz} \\ \tau_{\theta z} \end{Bmatrix} = \begin{bmatrix} Q_{11} & Q_{12} & 0 & 0 & 0 \\ Q_{12} & Q_{22} & 0 & 0 & 0 \\ 0 & 0 & Q_{66} & 0 & 0 \\ 0 & 0 & 0 & Q_{44} & 0 \\ 0 & 0 & 0 & 0 & Q_{55} \end{bmatrix} \left(\begin{Bmatrix} \varepsilon_{ss} \\ \varepsilon_{\theta\theta} \\ \gamma_{s\theta} \\ \gamma_{sz} \\ \gamma_{\theta z} \end{Bmatrix} - \begin{Bmatrix} \alpha_{ss}\Delta T \\ \alpha_{\theta\theta}\Delta T \\ 0 \\ 0 \\ 0 \end{Bmatrix} \right), \tag{15}$$

where σ_{ss} and $\sigma_{\theta\theta}$ are the normal stresses, $\tau_{s\theta}$ is the in-plane shear stress, τ_{sz} and $\tau_{\theta z}$ are the thickness shear stresses. ε_{ss} and $\varepsilon_{\theta\theta}$ are the normal strains, $\gamma_{s\theta}$ is in-plane shear strain and γ_{sz} and $\gamma_{\theta z}$ are the thickness shear strains. The coefficient of thermal expansion in the two principal directions (s, θ) is α_{ss} and $\alpha_{\theta\theta}$. ΔT is the temperature change from a stress-free state [28]. The suffixes used are based on the shell mid-surface coordinate system (s, θ, z). The stiffness coefficients are defined as

$$Q_{11} = Q_{22} = \frac{E_{\text{eff}}}{1 - v_{\text{eff}}^2}, \quad Q_{12} = \frac{v_{\text{eff}} E_{\text{eff}}}{1 - v_{\text{eff}}^2}, \quad Q_{44} = Q_{55} = Q_{66} = \frac{E_{\text{eff}}}{2(1 + v_{\text{eff}})}. \tag{16}$$

For a given power law index, the effective Young's Modulus E_{eff} (Eq. (4a)) and effective Poisson's ratio v_{eff} (Eq. (4b)) need to be evaluated in order to obtain the elastic coefficients Q_{ij}. Banks Sills et al. [27] have discussed the advantages and disadvantages of five functionally graded architectures for dynamic analysis. It was concluded that both the layered model and continuous model are suitable for the study of FGM. Each layer can be conceived as a homogeneous layer and follows the definition of the effective material properties as described in Eqs. (4a)–(4e). The methodology for computation of the reduced stiffness coefficients is incorporated into the semi-analytical finite element formulation to compute the stiffness matrix. The stiffness matrix is obtained from the strain energy; the element stiffness matrix corresponding to the mth harmonic is computed as follows:

$$\mathbf{k}_{\text{e}} = \int_A \mathbf{B}^{*\text{T}} \overline{\overline{\mathbf{D}}} \mathbf{B}^* r \, \text{d}s \, \text{d}\theta, \tag{17}$$

where $\mathbf{B}^*$ is the strain–displacement matrix (for details refer to Kadoli and Ganesan [26]) and $\overline{\overline{\mathbf{D}}}$ is the reduced stiffness coefficient. In $\overline{\overline{\mathbf{D}}}$, the extensional terms $\overline{\mathbf{A}}$, bending-extensional coupling

terms $\overline{\mathbf{B}}$ and bending terms $\overline{\mathbf{D}}$ are evaluated as follows:

$$\overline{\mathbf{A}} = \sum_{i\text{lay}=1}^{n\text{lay}} Q_{ij}(z_{i\text{lay}+1} - z_{i\text{lay}}), \tag{18a}$$

$$\overline{\mathbf{B}} = \frac{1}{2}\sum_{i\text{lay}=1}^{n\text{lay}} Q_{ij}(z^2_{i\text{lay}+1} - z^2_{i\text{lay}}), \tag{18b}$$

$$\overline{\mathbf{D}} = \frac{1}{3}\sum_{i\text{lay}=1}^{n\text{lay}} Q_{ij}(z^3_{i\text{lay}+1} - z^3_{i\text{lay}}), \tag{18c}$$

where $(i,\ j = 1, 2, 6)$. The details of various terms are given in Ref. [25]. The element stiffness matrix is assembled using the standard assembly procedure in finite element analysis to obtain the global stiffness matrix, $\mathbf{K}^{uu} = \sum \mathbf{k}_e$. The mass matrix is obtained from the kinetic energy of the FGM shell

$$\text{KE} = \frac{\rho}{2}\int_V (\dot{u}^2 + \dot{v}^2 + \dot{w}^2)\,\mathrm{d}V = \frac{\rho}{2}\int_V \mathbf{u}^{\mathrm{T}}\mathbf{u}\,\mathrm{d}V = \frac{1}{2}\,\mathbf{d}^{\mathrm{T}}\mathbf{m}_e\,\mathbf{d}, \tag{19}$$

where $\mathbf{u} = \overline{\mathbf{N}}\mathbf{d}$ and $\overline{\mathbf{N}}$ is the shape function matrix for a three-node quadratic line element expressed in terms of the isoparametric coordinate, described in Eq. (13), in which $\beta = -1$, 0 and $+1$ at nodes 1–3. $\mathbf{d}$ is a vector of nodal displacement and $\mathbf{m}_e$ is the element mass matrix given by

$$\mathbf{m}_e = \bar{\rho}_{\text{eff}}\int_A \overline{\mathbf{N}}^{\mathrm{T}}\overline{\mathbf{N}}\,\mathrm{d}A, \tag{20}$$

where

$$\bar{\rho}_{\text{eff}} = \sum_{i\text{lay}=1}^{n\text{lay}} \int_{h_{i\text{lay}}}^{h_{i\text{lay}+1}} \rho_{\text{eff}}\,\mathrm{d}z.$$

The computation of the mass matrix involves the use of effective density of the FGM shell as described in Eq. (4c). Now the formulation for linear static thermal buckling analysis of FGM conical shell is presented. For a discussion on the classical initial stability problems, the reader is referred to Zienkiewicz and Taylor [29]. The initial stiffness matrix (or geometric stiffness matrix) due to thermal loading is first evaluated. The initial stiffness matrix is evaluated as follows:

$$\mathbf{k}_{\sigma\mathrm{e}} = \int_A \mathbf{B}^{i^{\mathrm{T}}}\mathbf{N}^{*\mathrm{th}}\mathbf{B}^i\,\mathrm{d}A, \tag{21}$$

where $\mathbf{B}^i$ is the strain–displacement matrix based on strains due to large deformation [30] and $\mathbf{N}^{*\mathrm{th}}$ is a matrix of initial stress resultants N^{th}_{ij}, moment resultants M^{th}_{ij} and resultants shear forces $\bar{Q}^{\mathrm{th}}_{ij}$ due to temperature effects; this matrix is defined later. Assembling the element geometric stiffness matrix yields global geometric stiffness matrix, $\mathbf{K}^{uu}_{\sigma} = \sum \mathbf{k}_{\sigma e}$.

After computing the thermal load, the total stress resultants and moment resultants are determined [31] as follows:

$$\overline{\mathbf{N}}^{\mathrm{th}} = \overline{\overline{\mathbf{D}}}\boldsymbol{\varepsilon}_0 - \begin{Bmatrix} \mathbf{N}^{\mathrm{th}} \\ \mathbf{M}^{\mathrm{th}} \end{Bmatrix}, \tag{22}$$

where $\boldsymbol{\varepsilon}_0$ is the strain vector due to mechanical deflection arising from thermal loading. The initial stress resultants and moment resultants vector, $\overline{\mathbf{N}}^{\mathrm{th}}$, will be used to compose the initial stress resultants matrix $\mathbf{N}^{*\mathrm{th}}$. More details about stress resultant are provided in Ref. [25].

5. Temperature distribution across the thickness of the conical shell under steady-state heat conduction

The thermal analysis involving computation of thermal stresses, thermal buckling temperature, thermal static deflection and transient thermal response of FGM should consider heat transfer analysis. This is essential in order to account for material properties as a function of temperature.

A steady-state one-dimensional heat conduction analysis is considered to evaluate the temperature distribution across the thickness of the FGM shell based on specified temperature boundary conditions. A typical situation encountered can be in pipes conveying hot gases. The convective and radiation heat transfers are neglected. The finite element formulation used in the present work is based on the procedure discussed by Reddy [32].

The governing differential equation for steady-state radial direction heat conduction is

$$-\frac{\mathrm{d}}{\mathrm{d}z}\left(k(z)\frac{\mathrm{d}\hat{T}}{\mathrm{d}z}\right) = 0, \tag{23}$$

where k is the thermal conductivity of the material in kW/(m °C). The temperature boundary conditions are specified such that the T_i is the temperature on the inner surface and T_o is the temperature on the outer surface, which is normally the ambient temperature. Applying the variational principle to the governing equation, the following finite element equation to evaluate the temperature across the thickness due to heat conduction can be arrived at [30]:

$$\mathbf{K}_{\mathrm{con}}\hat{\mathbf{T}} = 0. \tag{24}$$

The above equation is solved given the temperature at the inner surface and outer surface to obtain the temperature distribution, $\hat{\mathbf{T}}$, across the thickness. This procedure has been extended to compute the temperature distribution across the wall of the FGM shell by accounting for the material properties as a function of temperature. An iterative procedure is followed in order to obtain a converged temperature distribution in the subsequent studies. The procedure is well understood through the flow chart reported in Ref. [25], and hence not reported here.

6. Results and discussion

In this section the authors presented the thermal buckling, and free vibration behaviors are presented for a functionally graded conical shell having different semi-vertex angles at the apex.

Different FGM materials made up of ceramic and metal combinations are analyzed to see relative merit among them.

6.1. Thermal buckling studies

6.1.1. Convergence study

A convergence study is taken up in order to determine the finite element mesh and suitable number of homogeneous layers to represent the FGM truncated conical shell thickness. An FGM conical shell composed of SUS304-Al_2O_3 with $r/h = 292$ and $l/r = 1.04$, having a mean radius equal to 0.876 m with a semi-vertex angle (β_{sv}) of 10° is considered for the convergence study. The conical shell is clamped–clamped for both circular edges by arresting all the DOF. Four finite element mesh models are considered with 10, 20, 30 and 40 for element convergence and 5, 10, 20 and 25 layer models for choice of layer-wise convergence across the thickness, accounted for in the initial stage of the study. The converged lowest critical buckling temperatures are reported in Tables 1 and 2 for different power law indexes for choice of element and layer, respectively. The percentage difference between buckling temperature predicted by 30 element models and 40

Table 1
Convergence study for the choice of number of elements for FGM conical shell having semi-vertex angle 10°

Power law index n	Critical thermal buckling temperature $T_{critical}$ (°C)			
	10 elements	20 elements	30 elements	40 elements
0.0 (metal rich)	592.85 (9,1)	589.22 (9,1)	588.15 (9,1)	588.11 (9,1)
0.5	630.25 (9,1)	627.11 (9,1)	626.05 (9,1)	626.00 (9,1)
1.0	910.58 (9,1)	902.44 (9,1)	901.35 (9,1)	901.32 (9,1)
5.0	999.94 (9,1)	994.94 (9,1)	993.87 (9,1)	993.81 (9,1)
10.0	1091.47 (9,1)	1085.15 (9,1)	1084.08 (9,1)	1084.05 (9,1)
15.0	1140.92 (9,1)	1135.92 (9,1)	1134.78 (9,1)	1134.70 (9,1)
1000.0 (ceramic)	1253.81 (9,1)	1246.81 (9,1)	1245.78 (9,1)	1245.78 (9,1)

Table 2
Convergence study for the choice of number of layers for FGM conical shell thickness having semi-vertex angle 10°

Power law index n	Critical thermal buckling temperature $T_{critical}$ (°C)			
	5 layers	10 layers	20 layers	25 layers
0.0 (metal rich)	590.12	589.34	588.22	588.20
0.5	628.00	629.25	626.11	626.09
1.0	905.98	903.25	901.44	901.39
5.0	998.25	994.58	993.94	993.94
10.0	1089.48	1086.56	1084.15	1084.08
15.0	1143.45	1138.55	1134.92	1134.92
100.0	1243.25	1241.25	1240.04	1240.01
1000.0 (ceramic)	1248.45	1246.89	1245.81	1245.98

element models is less than as compared to 10 and 20 element models. In case of the layer-wise mesh model there is quite good convergence for 20 layers and 25 layers. In addition, it is noticed that the circumferential mode number remains unchanged from model to model. Based on the above observation and from the point of view of lesser computational time, it is reasonable to use 30 elements and 20 layers across the thickness.

6.1.2. Validation

As there is no literature available on thermal buckling of FGM truncated conical shells, the results are validated with an isotropic conical shell [6] by setting the value of the power law index equal to zero in the present formulation.

An attempt has been made to validate the buckling result with the experimental results reported by Lu and Chang [6]. Details of the truncated conical shell considered for validation are as follows: ratio of height (H) of the shell to radius (R) is equal to 2.0; ratios of radius (R) to thickness of shell (h) are equal to 200,400,600 and 800; semi-vertex angles (β_{sv}) equal to 10° and 30°. Table 3 shows the comparison of the thermal buckling strains reported by Lu and Chang [6] and those computed from the present method. Even though the absolute magnitude of thermal buckling strains does not agree too well, the trends are in good unison. Lu and Change [7] do report that the experimental values are higher by about 20–30% than the theoretical values.

In addition to ensuring the accuracy of the proposed finite element model, thermal buckling results obtained by the computer code for FGM truncated conical shell were compared with those reported by Ravikiran [22] for FGM cylindrical shell by incorporating semi-vertex angle of the conical shell to 0° (equivalent to the cylindrical shell) and given in Table 4. From Table 4 it is seen that there is excellent correlation between the results.

Table 3
Validation of critical buckling strains for a special case of isotropy

R/H	Semi-vertex angle $\beta_{sv} = 10^\circ$			Semi-vertex angle $\beta_{sv} = 30^\circ$		
	Present	Lu and Chang [7]	% error	Present	Lu and Chang [7]	% error
200	3.00	2.4	25.34	2.98	2.2	35.52
400	1.51	1.2	26.53	1.47	1.08	36.21
600	1.00	0.787	27.06	0.96	0.68	41.78
800	0.736	0.600	22.82	0.71	0.5	42.17

Table 4
Validation of critical buckling temperature ($T_{critical}$) in °C for cylindrical shell

Power law index n	Present	RaviKiran [22]
0.0	598.98	598.99
1.00	714.62	714.65
1000.0	1271.07	1272.06

SUS304-Al_2O_3 ($r/h = 100$ and $l/r = 1.0438$).

Having validated the model, an attempt has been made to study the thermal buckling behavior of the FGM truncated conical shell having different semi-vertex angles. The evaluation of the thermal buckling temperature is based on the classical stability equation involving the structural stiffness matrix, $\mathbf{K}^{uu}$, and initial stiffness matrix, $\mathbf{K}_{\sigma}^{uu}$. The buckling eigenvalues and buckling mode shapes are computed using the simultaneous iteration technique. A typical configuration of the functionally graded truncated conical shell is assumed to be ceramic rich on the inner surface and metal rich on the outer surface. The material properties are dependent on temperature. An iterative procedure is implemented for the computation of the thermal buckling temperature. In addition, the thermal buckling study has been done by accounting for the variation of material properties with respect to temperature. As the problem becomes nonlinear, an iterative procedure has been adopted. The converged value of buckling temperature has been reported in a subsequent table. The overall procedure followed for the determination of the converged thermal buckling temperature is explained in detail in Ref. [25], and hence is not repeated here. Thermal buckling analysis of the FGM shell is carried out in two steps. First, the heat conduction equation is solved for temperature distribution across the thickness of the shell, having specified the temperature boundary condition. Variation of temperature along the length of the shell is assumed to be negligible. The thermal material property is dependent on temperature, and hence a converged temperature distribution is obtained. Based on the converged temperature distribution, the mechanical and thermal properties are evaluated. The error between the critical buckling temperature obtained between the previous step and the new step is chosen to be less than or equal to 0.005. The loop for checking the convergence of buckling temperature is initiated by setting a large error. The first critical buckling temperature obtained is set as the old buckling temperature. This temperature is now set as the specified temperature on the inner surface of the conical shell and the outer surface of the conical shell is always set to an ambient temperature of 27 °C.

6.2. *Thermal buckling studies by accounting for different temperature loads*

Having validated the present formulation for the isotropic (pure metal) truncated conical shell to a certain extent in the present study, an attempt has been made to find out the thermal buckling behaviors made up of a mixture of metal and ceramic FGM pairs with different material combinations. In the present two combinations, SUS304-Al_2O_3 and Ti–6Al–4V–Al_2O_3 are used. The following temperature distribution profile cases across the thickness for $l/r = 1.0438$, $r/h = 292$ and clamped–clamped boundary conditions of the shell have been investigated:

1. Assuming uniform temperature distribution (Case A),
2. Linear temperature across the thickness (Case B),
3. Temperature distribution across the thickness considering temperature-dependent material properties and follows iterative procedure [25].

Results are shown in Tables 5 and 6 for the two FGM material pair combinations.

It is found from Table 5 that the thermal buckling temperatures obtained by linear and nonlinear variations across the thickness are higher than those of uniform temperature. This behavior is as expected. In addition, it is found that in the case of SUS304-Al_2O_3 the thermal buckling values obtained considering material property variation with respect to temperature are,

Table 5
Critical buckling temperature $T_{critical}$ for truncated SUS304-Al_2O_3 FGM conical shells for different power law indexes

Power law index n	$\beta_{sv} = 15.0$			$\beta_{sv} = 30.0$		
	Case A	Case B	Case C	Case A	Case B	Case C
0.0	151.11	261.54	248.33	140.74	242.45	231.55
0.5	183.25	330.78	262.53	170.29	306.12	244.74
1.0	202.89	375.91	292.31	188.31	347.53	272.13
5.0	254.20	477.46	400.17	235.68	441.27	372.24
10.0	270.86	500.96	444.35	251.00	462.87	413.18
15.0	278.18	509.96	464.76	257.69	471.08	432.15
100.0	294.95	527.87	508.08	273.00	487.31	472.34
1000.0	296.35	529.11	510.42	274.28	488.42	474.52

$l/r = 1.0438$, $r/h = 292$ and clamped–clamped boundary conditions.

Table 6
Critical buckling temperature $T_{critical}$ for truncated Ti–6Al–4V–Al_2O_3 FGM conical shells for different power law indexes

Power law index n	$\beta_{sv} = 15.0$			$\beta_{sv} = 30.0$		
	Case A	Case B	Case C	Case A	Case B	Case C
0.0	198.18	348.22	270.53	184.01	322.14	254.99
0.5	225.63	370.31	282.30	209.32	342.48	264.81
1.0	236.93	391.49	379.51	219.90	362.30	353.79
5.0	265.74	458.75	427.00	246.58	424.50	397.51
15.0	282.14	497.30	450.94	261.48	459.66	419.49
1000.0	296.35	529.11	510.94	274.28	488.42	474.52

$l/r = 1.0438$, $r/h = 292$ and clamped–clamped boundary conditions.

in general, lower than those obtained without accounting for material property variation. In general, it is expected that for the isotropic case, $T_{critical}$ of shell subjected to linearly varying temperature is twice that obtained for the shell subjected to uniform temperature. In contrast, such a trend is not observed in the case of an FGM shell even for $n = 0.0$ and 1000.0. In this case, the $T_{critical}$ value obtained for a shell with varying temperature is not twice that of the shell subjected to uniform temperature, but lower than the $2T_{critical}$. This can be due to the fact that temperature-dependent material properties have been used in the present study. A similar discussion holds good for another type of FGM material pair Ti–6Al–4V–Al_2O_3.

A further thermal buckling study has been carried out by accounting for converged temperature distribution and thereby material properties and follows the iterative procedure as explained in Ref. [25].

6.3. Thermal buckling parameter studies

The lowest or critical buckling temperature of Ti–6Al–4V–Al_2O_3 with the associated mode for different semi-vertex angles is listed in Table 7 for different r/h ratios. Here power law index

Table 7
Critical buckling temperature $T_{critical}$ for truncated Ti–6Al–4V-Al_2O_3 FGM conical shells for different power law indexes

Power law index n	$r/h = 100.0$								$r/h = 200.0$							
	$\beta_{sv} = 15.0$		$\beta_{sv} = 30.0$		$\beta_{sv} = 45.0$		$\beta_{sv} = 60.0$		$\beta_{sv} = 15.0$		$\beta_{sv} = 30.0$		$\beta_{sv} = 45.0$		$\beta_{sv} = 60.0$	
	$T_{critical}$	Mode	$T_{critical}$	Mode	$T_{critical}$	Mode	$T_{critical}$	Mode	$T_{critical}$	Mode	$T_{critical}$	Mode	$T_{critical}$	Mode	$T_{critical}$	Mode
0.0	490.61	(9,1)	427.27	(8,1)	345.84	(6,1)	241.66	(10,1)	348.39	(12,1)	329.78	(11,1)	302.93	(9,1)	298.77	(14,1)
0.5	491.41	(9,1)	424.89	(8,1)	339.11	(6,1)	231.99	(10,1)	345.25	(12,1)	325.58	(11,1)	299.52	(9,1)	392.24	(14,1)
1.0	548.28	(9,1)	470.51	(8,1)	371.27	(6,1)	249.90	(10,1)	374.37	(12,1)	351.88	(11,1)	320.04	(9,1)	314.88	(14,1)
5.0	810.52	(9,1)	678.40	(8,1)	517.03	(6,1)	332.29	(10,1)	521.26	(12,1)	485.83	(11,1)	436.59	(9,1)	429.76	(14,1)
10.0	929.38	(9,1)	772.44	(8,1)	584.75	(6,1)	373.22	(10,1)	589.35	(12,1)	548.72	(11,1)	492.25	(9,1)	484.84	(14,1)
15.0	984.07	(9,1)	816.58	(8,1)	617.70	(6,1)	393.94	(10,1)	622.34	(12,1)	579.62	(11,1)	519.89	(9,1)	512.13	(14,1)
1000.0	1111.62	(9,1)	921.45	(8,1)	698.24	(6,1)	445.82	(10,1)	702.84	(12,1)	655.32	(11,1)	588.0	(9,1)	579.84	(14,1)
	$r/h = 292.0$								$r/h = 584.0$							
0.0	270.53	(14,1)	254.99	(13,1)	232.95	(10,1)	229.48	(16,1)	163.48	(20,1)	153.39	(18,1)	138.88	(14,1)	137.44	(23,1)
0.5	260.98	(14,1)	245.34	(13,1)	222.98	(10,1)	219.14	(17,1)	154.10	(20,1)	144.28	(18,1)	130.48	(14,1)	130.48	(23,1)
1.0	282.30	(14,1)	264.81	(13,1)	239.80	(11,1)	235.31	(17,1)	175.37	(20,1)	165.72	(18,1)	149.52	(14,1)	147.25	(23,1)
5.0	379.51	(15,1)	353.79	(13,1)	317.03	(11,1)	311.48	(17,1)	208.84	(21,1)	194.31	(18,1)	173.59	(14,1)	171.80	(23,1)
10.0	427.00	(15,1)	397.51	(13,1)	355.90	(11,1)	349.78	(17,1)	233.06	(21,1)	216.51	(18,1)	193.08	(14,1)	191.23	(23,1)
15.0	450.94	(15,1)	419.49	(13,1)	375.67	(11,1)	369.22	(17,1)	245.64	(21,1)	228.05	(18,1)	203.23	(14,1)	201.34	(23,1)
1000.0	510.94	(15,1)	474.52	(13,1)	424.67	(10,1)	418.32	(17,1)	277.79	(21,1)	257.66	(18,1)	229.34	(14,1)	227.56	(23,1)

$l/r = 1.0438$ and clamped–clamped boundary conditions.

$n = 0.0$ corresponds to an isotropic shell with properties corresponding to that of metal and $n = 1000.0$ corresponds to a cylindrical shell purely of ceramic material. The power law index value n other than two extreme values governs the distribution of properties of metal–ceramic mixture in the FGM shell. Variation of the composition of metal and ceramic is linear for the power law index $n = 1.0$. From Table 7 it is found that as the value of the power law index increases, the critical buckling temperature increases as it approaches the homogeneous ceramic composition. The only exception is when $n = 0.5$, which has a lower value.

Such a trend is expected because the coefficient of thermal expansion of ceramic is lower than that of metal. In addition, it is observed that thermal buckling temperature decreases with an increase in the semi-vertex angle for $l/r = 1.0$. From Table 7, it is clear that as the r/h ratio is increased, the critical buckling temperature decreases. This trend is also expected as the thickness reduces. In addition, it is noticed that the lowest circumferential buckling mode decreases as the semi-vertex angle of the cone increases, but for cone angle $= 60^\circ$ it is higher. This behavior holds good for all r/h ratios. As the n is increased from 1.0 to 5.0, there is a sudden rise in temperature when compared to other cases. Another observation from Table 7 is that when the thickness of the shell reduces, the buckling temperature decreases as expected.

To further understand the effect on magnitude of lowest or critical buckling temperature due to semi-vertex angle, a study has been carried out by plotting the stress resultant along the meridian of the FGM shell for special cases $n = 1.0$ with different semi-vertex angle as shown in Fig. 3. The meridional stress resultant N_{ss} decreases for $n = 1.0$ as the distance from the small end radius of the shell increases, and is low in magnitude (i.e. less compressive) close to the big end radius of the shell as shown in Fig. 3(a). The increase in the gradient of the stress resultant is large for the truncated conical shell with 60° semi-vertex angle, then 45° and subsequently 30°, 15° and 0°. Semi-vertex angle 0° represents the cylindrical shell. Fig. 3(b) illustrates the distribution of hoop stress resultants $N_{\theta\theta}$ for $n = 1.0$. The hoop stress resultants are concentrated over a small length of the

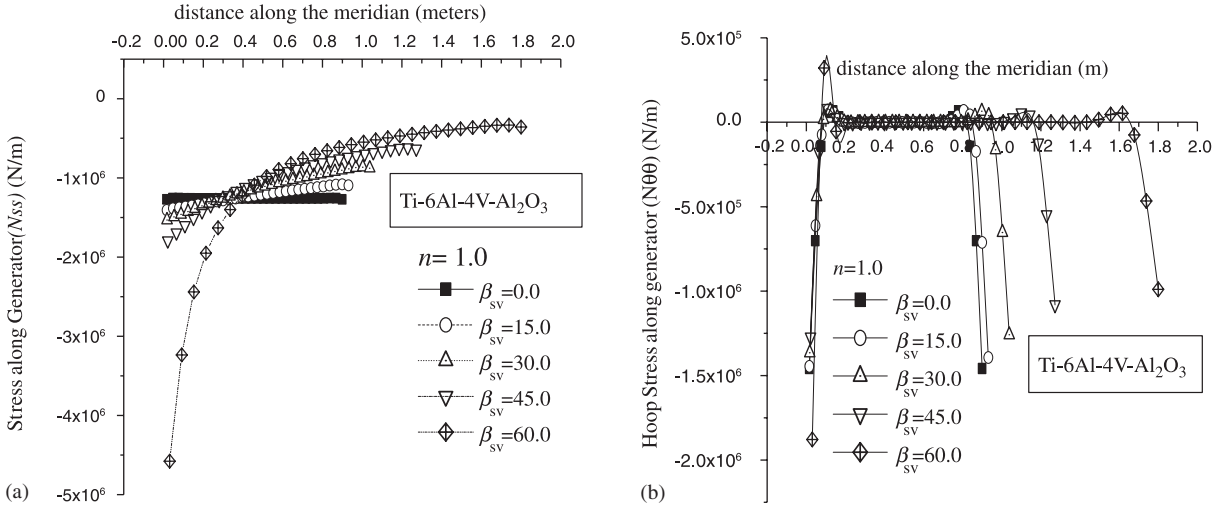

Fig. 3. (a, b) Distribution of stress resultant for truncated FGM conical shells Ti–6Al–4V–Al_2O_3 for power law index $n = 1$.

meridian close to the clamp of the shell and are very large in magnitude. The magnitude of the hoop stress resultants decreases drastically from the clamped edges of the shell and remains constant over a large length of the meridian. From the study on the distribution and magnitude of stress resultants, it is evident that the magnitude of meridional stress resultants is likely to provide an indication of the critical buckling temperature. For $\beta_{sv} = 60$ has a large magnitude (compressive in nature) of meridional stress resultant, there exists, more or less, half the length of the shell, followed by truncated conical shell $\beta_{sv} = 45^\circ$, 30° and 15°. Thus, the truncated conical shell with $\beta_{sv} = 60$ has a low thermal buckling temperature compared to the shell with $\beta_{sv} = 45^\circ$, 30° and 15°.

The critical thermal buckling study has been carried out for different FGM material pairs for selected r/h ratios. Another pair of FGM conical shell made up of SUS304-Si_3N_4 is considered for the evaluation of critical buckling temperature. The results are tabulated in Table 8. From Table 8 it is seen that as n increases, the critical thermal buckling temperature increases. The critical buckling temperatures for SUS304-Si_3N_4 are high and increase marginally for n ranging from 5 to 1000. On the other hand, for $n = 0$ the value of $T_{critical}$ is small, since larger the coefficient of thermal expansion, lower the buckling temperature. For materials with a high coefficient of thermal expansion (by consideration of the temperature gradient), the strains due to temperature rise dominate the mechanical strains. Hence, the stresses due to temperature effects are larger when compared to the stresses from mechanical deflection. This will lead to high initial compressive stresses in the shell, which is likely to cause the shell to buckle at lower thermal loading. Further, the buckling study has been carried out for another pair of FGM truncated conical shells namely SUS304-Al_2O_3; results are shown in Table 9. For SUS304-Al_2O_3 FGM shells the critical buckling temperatures are high for ceramic composition, i.e. $n = 1000$. The critical buckling temperatures increase with increase in power law index. When considering ceramics like Si_3N_4 and Al_2O_3, in combination with SUS304, the FGM shells are best suited for higher operating temperature since these exhibit higher buckling temperatures.

7. Critical thermal buckling temperature of FGM truncated conical shell based on average coefficient of thermal expansion

In this section, an attempt has been made to look for an alternate procedure for the determination of critical thermal buckling temperature for FGM truncated shells fabricated with various power law index n. In general, it is easy to obtain the critical thermal buckling temperature of the homogeneous isotropic ceramic or metallic FGM shell. Following the assumptions that (i) geometrical parameters of the FGM shell and isotropic shell are the same, (ii) for a given geometry, thermal strains at the critical buckling temperature remain the same for the FGM shell and the isotropic shell and (iii) knowing the critical buckling temperature of isotropic shell referred to as reference temperature, a method is proposed to evaluate the thermal buckling temperature of an FGM shell for a given n. Since an FGM shell is assumed to consist of many homogeneous isotropic lamina, it is appropriate to represent the coefficient of thermal expansion of the FGM shell for a given power law index as an average of the effective coefficient thermal expansion computed based on Eq. (4e). Then

$$\varepsilon^{th}\big|_{\underline{n}\gg 100.0} = \varepsilon^{th}\big|_{0.0\leqslant \underline{n} \leqslant 100.0} \text{ or } (\alpha_{ref}\,\Delta T_{ref})_{\underline{n}\gg 100.0} = (\alpha_{avg}\,\Delta T_{cri})_{0.0\leqslant \underline{n} \leqslant 100.0}.$$

Table 8
Critical buckling temperature $T_{critical}$ for truncated SUS304-Si_3N_4 FGMs conical shells for different power law indexes

Power law index n	$r/h = 100.0$								$r/h = 200.0$							
	$\beta_{sv} = 15.0$		$\beta_{sv} = 30.0$		$\beta_{sv} = 45.0$		$\beta_{sv} = 60.0$		$\beta_{sv} = 15.0$		$\beta_{sv} = 30.0$		$\beta_{sv} = 45.0$		$\beta_{sv} = 60.0$	
	$T_{critical}$	Mode	$T_{critical}$	Mode	$T_{critical}$	Mode	$T_{critical}$	Mode	$T_{critical}$	Mode	$T_{critical}$	Mode	$T_{critical}$	Mode	$T_{critical}$	Mode
0.0	588.22	(9,1)	551.34	(8,1)	497.82	(6,1)	491.99	(10,1)	338.53	(12,1)	316.54	(11,1)	285.09	(9,1)	279.86	(14,1)
0.2	680.82	(9,1)	638.34	(8,1)	576.25	(6,1)	567.71	(10,1)	391.55	(12,1)	365.91	(11,1)	329.32	(9,1)	322.48	(14,1)
0.5	811.47	(9,1)	760.67	(8,1)	686.15	(6,1)	674.01	(10,1)	463.87	(12,1)	432.87	(11,1)	388.85	(9,1)	380.03	(14,1)
1.0	965.68	(9,1)	905.77	(8,1)	816.95	(6,1)	801.22	(10,1)	549.21	(12,1)	511.68	(11,1)	458.38	(9,1)	447.73	(14,1)
5.0	1125.74	(9,1)	1064.40	(8,1)	966.36	(6,1)	951.57	(10,1)	658.59	(12,1)	613.91	(11,1)	551.07	(9,1)	541.17	(14,1)
10.0	1126.75	(9,1)	1061.02	(8,1)	964.55	(6,1)	952.41	(10,1)	660.95	(12,1)	616.77	(11,1)	554.27	(9,1)	545.69	(14,1)
15.0	1123.96	(9,1)	1058.61	(8,1)	962.67	(6,1)	951.54	(10,1)	660.46	(12,1)	616.97	(11,1)	554.58	(9,1)	545.78	(14,1)
1000	1118.88	(9,1)	1054.10	(8,1)	958.42	(6,1)	950.14	(10,1)	658.74	(12,1)	617.98	(11,1)	554.98	(9,1)	545.81	(14,1)
	$r/h = 292.0$								$r/h = 584.0$							
0.0	248.33	(14,1)	231.55	(13,1)	207.95	(10,1)	203.99	(16,1)	138.63	(20,1)	129.19	(18,1)	115.76	(14,1)	114.26	(23,1)
0.2	286.47	(14,1)	266.90	(13,1)	239.40	(10,1)	234.38	(16,1)	158.60	(20,1)	147.59	(18,1)	131.95	(14,1)	130.02	(23,1)
0.5	337.44	(14,1)	313.95	(13,1)	281.04	(10,1)	274.55	(16,1)	184.58	(20,1)	171.45	(18,1)	152.86	(14,1)	150.43	(23,1)
1.0	396.80	(14,1)	368.44	(13,1)	329.15	(10,1)	321.22	(16,1)	214.24	(20,1)	198.60	(18,1)	176.63	(14,1)	173.85	(23,1)
5.0	477.96	(15,1)	444.51	(13,1)	397.72	(10,1)	389.72	(16,1)	259.26	(20,1)	240.17	(18,1)	213.66	(14,1)	211.20	(23,1)
10.0	481.43	(15,1)	448.01	(13,1)	401.36	(10,1)	394.30	(16,1)	262.58	(20,1)	243.40	(18,1)	216.72	(14,1)	214.62	(23,1)
15.0	481.81	(15,1)	448.43	(13,1)	401.80	(10,1)	395.23	(16,1)	263.22	(20,1)	244.07	(18,1)	217.38	(14,1)	215.47	(23,1)
1000	481.56	(15,1)	448.14	(13,1)	401.59	(10,1)	396.28	(16,1)	263.64	(20,1)	244.65	(18,1)	218.01	(14,1)	216.53	(23,1)

$l/r = 1.0438$ and clamped–clamped boundary conditions.

Table 9
Critical buckling temperature $T_{critical}$ for truncated SUS304-Al_2O_3 FGM conical shells for different power law indexes

Power law index n	$r/h = 100.0$								$r/h = 200.0$							
	$\beta_{sv} = 15.0$		$\beta_{sv} = 30.0$		$\beta_{sv} = 45.0$		$\beta_{sv} = 60.0$		$\beta_{sv} = 15.0$		$\beta_{sv} = 30.0$		$\beta_{sv} = 45.0$		$\beta_{sv} = 60.0$	
	$T_{critical}$	Mode	$T_{critical}$	Mode	$T_{critical}$	Mode	$T_{critical}$	Mode	$T_{critical}$	Mode	$T_{critical}$	Mode	$T_{critical}$	Mode	$T_{critical}$	Mode
0.0	588.22	(9,1)	551.34	(8,1)	497.82	(6,1)	491.99	(10,1)	338.53	(12,1)	316.54	(11,1)	285.09	(9,1)	279.86	(14,1)
0.5	626.11	(9,1)	586.94	(8,1)	529.36	(6,1)	520.35	(10,1)	358.69	(12,1)	335.08	(11,1)	301.57	(9,1)	295.11	(14,1)
1.0	701.44	(9,1)	657.39	(8,1)	592.81	(6,1)	581.70	(10,1)	400.50	(12,1)	373.71	(11,1)	335.57	(9,1)	328.73	(14,1)
5.0	973.94	(9,1)	912.08	(8,1)	822.21	(6,1)	808.27	(10,1)	552.11	(12,1)	514.23	(11,1)	461.27	(9,1)	452.80	(14,1)
10.0	1084.15	(9,1)	1014.52	(8,1)	913.77	(6,1)	900.385	(10,1)	613.05	(12,1)	571.04	(11,1)	512.22	(9,1)	503.74	(14,1)
15.0	1134.72	(9,1)	1061.41	(8,1)	955.38	(6,1)	942.43	(10,1)	641.13	(12,1)	597.28	(11,1)	535.73	(9,1)	527.24	(14,1)
100.0	1240.04	(9,1)	1159.15	(8,1)	1042.17	(6,1)	1030.48	(10,1)	699.65	(12,1)	652.34	(11,1)	585.32	(9,1)	577.00	(14,1)
1000	1245.81	(9,1)	1164.33	(8,1)	1046.79	(6,1)	1035.38	(10,1)	702.84	(12,1)	655.32	(11,1)	588.00	(9,1)	579.84	(14,1)
	$r/h = 292.0$								$r/h = 584.0$							
0.0	248.33	(14,1)	231.55	(13,1)	207.95	(10,1)	203.99	(16,1)	138.63	(20,1)	129.19	(18,1)	115.76	(14,1)	114.26	(23,1)
0.5	262.53	(14,1)	244.74	(13,1)	219.74	(10,1)	215.01	(16,1)	146.58	(20,1)	136.63	(18,1)	122.53	(14,1)	120.78	(23,1)
1.0	292.31	(15,1)	272.13	(13,1)	244.14	(10,1)	238.74	(16,1)	162.11	(20,1)	150.92	(18,1)	135.13	(14,1)	133.21	(23,1)
5.0	400.17	(15,1)	372.24	(13,1)	333.35	(10,1)	326.67	(17,1)	218.64	(20,1)	202.87	(18,1)	180.93	(14,1)	178.82	(23,1)
10.0	444.35	(15,1)	413.18	(13,1)	369.88	(10,1)	363.13	(17,1)	242.13	(20,1)	224.55	(18,1)	200.07	(14,1)	197.95	(23,1)
15.0	464.76	(15,1)	432.15	(13,1)	386.84	(10,1)	380.10	(17,1)	253.09	(20,1)	234.72	(18,1)	209.05	(14,1)	206.96	(23,1)
100.0	508.08	(15,1)	472.34	(13,1)	422.74	(10,1)	416.29	(17,1)	276.51	(20,1)	256.47	(18,1)	228.28	(14,1)	226.31	(23,1)
1000.0	510.42	(15,1)	474.52	(13,1)	424.67	(10,1)	418.32	(17,1)	277.79	(20,1)	257.66	(18,1)	229.34	(14,1)	227.37	(23,1)

$l/r = 1.0438$ and clamped–clamped boundary conditions.

With the above relation, the evaluation of the critical buckling temperature for a given value of power law index n is investigated. The left-hand side of the above equation represents the critical thermal strain of a homogeneous isotropic material, ceramic or metallic, which is equivalent to an FGM shell with $n = 1000$ or 0.0, α_{ref} is the coefficient of thermal expansion of the isotropic shell and ΔT_{ref} refers to reference temperature, which is equal to the critical buckling temperature for the isotropic shell. Given the critical buckling temperature for a homogeneous isotropic shell, and evaluating the average coefficient of thermal expansion α_{avg} for a given power law index say, $n = 0.05$ or 0.1 and so on, the above relation will yield the critical thermal buckling temperature for the FGM shell corresponding to the choice of n. The above procedure is implemented for the case of FGM shells composed of SUS304-Al_2O_3 constituent materials. For a shell with $l/r = 1.0438$, two ratios of r/h are considered. The results of the same are listed in Table 10 along with the percentage error in the estimation of the critical buckling temperature by this alternate procedure. From Table 10, it is seen that the percentage error is higher for first few n. This is because buckling temperatures are evaluated at ΔT_{ref} which is pure ceramic. It is to be noted that the buckling temperatures evaluated by this procedure depend on the reference temperature chosen as well as n. This procedure can be used for the estimation of the critical buckling temperature during the preliminary design stage of an FGM shell. Thus, initially, this helps in making a proper choice of the power law index of the FGM shell, and subsequently the iterative procedure can be used to determine the buckling temperature.

8. Free vibration frequency studies of the truncated conical shell

Free vibration characteristics are presented for clamped–clamped FGM shells with various values of the power law index. Apart from the free vibration studies, the effect of temperature on the free vibration natural frequencies of FGM shells is also investigated.

8.1. Validation of natural frequencies for functionally graded conical shells

Once again, there is no literature available on the free vibration studies of FGM truncated conical shells. An attempt has been made to validate the present formulations for the isotropic case reported by Lakis et al. [13] by incorporating the value of power law index $n = 0.0$. The characteristics of the shell under study for validation purpose are $\beta_{sv} = 14.2^\circ$, $t = 2.56 \times 10^{-4}$ m, $\rho = 7800\,\text{kg/m}^3$, $E = 200 \times 10^9$ Pa, $v = 0.3$. Fig. 4 gives the nondimensional frequency (Ω) with first 20 circumferential mode numbers.

After validating, the present formulation studies have been carried out for FGM conical shell combinations made up of SUS304-Si_3N_4 and Ti–6Al–4V–Al_2O_3. The first axial mode frequencies associated with first 20 circumferential modes for a clamped–clamped boundary condition are presented in Figs. 5 and 6, respectively. The frequency characteristic is typical of homogeneous isotropic or orthotropic shells, depicting a bathtub curve. The frequency characteristics do not change with the power law index and follow the same behavior. The influence of the power law index is mainly to change the magnitude of the first axial mode frequency. As the power law index increases, the frequencies increase. The frequencies are low for power law index $n = 0.0$ and high for $n = 1000$. This fact can be understood easily, as the Young's Modulus of ceramics, Si_3N_4 and

Table 10
Comparison of critical buckling temperature $T_{critical}$ based on average coefficient of thermal expansion (ACTE) and iterative computational procedure

Power law index n	$\beta_{sv} = 15.0$			$\beta_{sv} = 30.0$			$\beta_{sv} = 45.0$			$\beta_{sv} = 60.0$		
	Actual procedure	ACTE	% error	Actual procedure	ACTE	% error	Actual procedure	ACTE	% error	Actual procedure	ACTE	% error
0.0	588.22	459.40	21.86	551.34	434.26	21.23	497.82	397.62	20.12	491.99	394.02	19.91
0.5	626.11	563.39	10.0	586.94	533.55	9.0	529.36	489.26	7.5	520.35	484.88	6.81
1.0	701.44	659.28	6.0	657.39	623.14	5.1	592.81	569.67	3.9	581.70	564.39	2.97
5.0	973.94	992.85	1.9	912.08	931.48	2.0	822.21	842.11	2.4	808.27	833.38	3.1
10.0	1084.15	1106.92	2.1	1014.52	1036.18	2.1	913.77	933.73	2.1	900.385	923.76	2.5
15.0	1134.72	1152.79	1.5	1061.41	1078.32	1.5	955.38	970.64	1.6	942.43	960.17	1.8
100.0	1240.04	1240.12	0.0	1159.15	1159.03	0.0001	1042.17	1042.03	0.0001	1030.48	1030.68	0.0001
1000.0	1245.81	1245.81	0.0	1164.33	1164.33	0.0	1046.79	1046.79	0.0	1035.38	1035.38	0.0

Reference ΔT_{ref} is ceramic. SUS304-Si_3N_4 FGM shell with $r/h = 100.0$ and $l/r = 1.0438$.

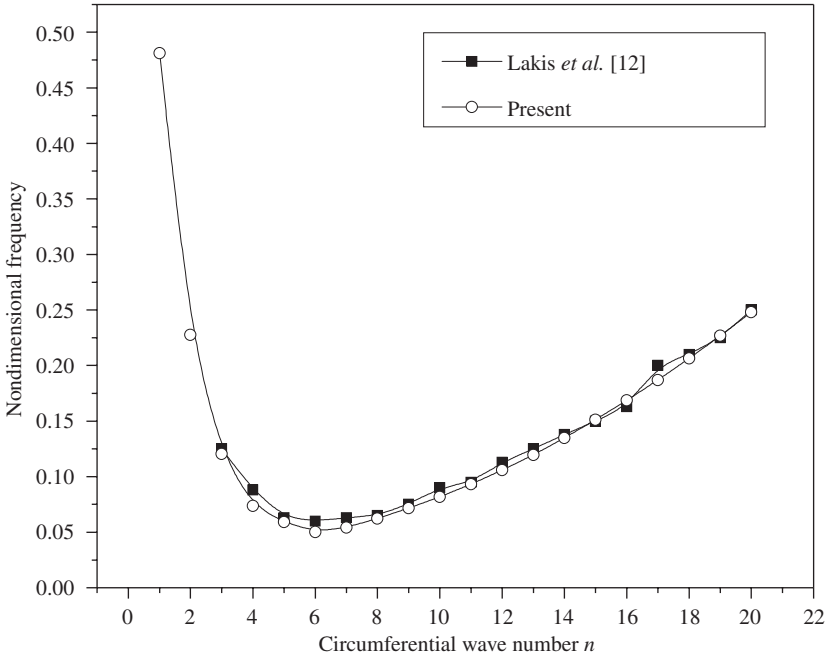

Fig. 4. Validation of natural frequency of the conical shell.

Al_2O_3, is much higher compared to their metal counterpart. The power law index does not have a great influence in shifting the associated circumferential mode number for the lowest of the first axial mode frequency. As the semi-vertex angle of the truncated conical shell increases, the frequency reduces.

8.2. *Effect of temperature on frequency behavior of truncated FGM conical shells*

In order to understand the behavior of the natural frequency variation with respect to temperature, studies have been carried out on SUS304-Si_3N_4 FGM truncated conical shells. The FGM shells are ceramic rich on their inner surface. This configuration is best suited for shells conveying fluids and hot gases at a high temperature. The evaluation of the natural frequencies is conducted based on the specified temperature on the inner surface and the outer surface is always at ambient temperature. The temperature on the inner surface is varied in steps of suitable increments and the highest temperature for the study is limited to the lowest thermal buckling temperature for the shell geometry and FGM composition (or power law index n). The lowest buckling temperatures for SUS304-Si_3N_4 FGM shell with a geometry of $l/r = 1.048$ and $r/h = 292$ for various power law indices are listed in Table 8. Study has been carried out for different semi-vertex angles. Now given the temperature boundary condition on the inner surface and ambient temperature on the outer surface, the converged temperature distribution is obtained. Based on the converged temperature distribution, the thermal load vector, total initial stresses and hence the geometric stiffness matrix are computed. This initial stiffness matrix is added to the

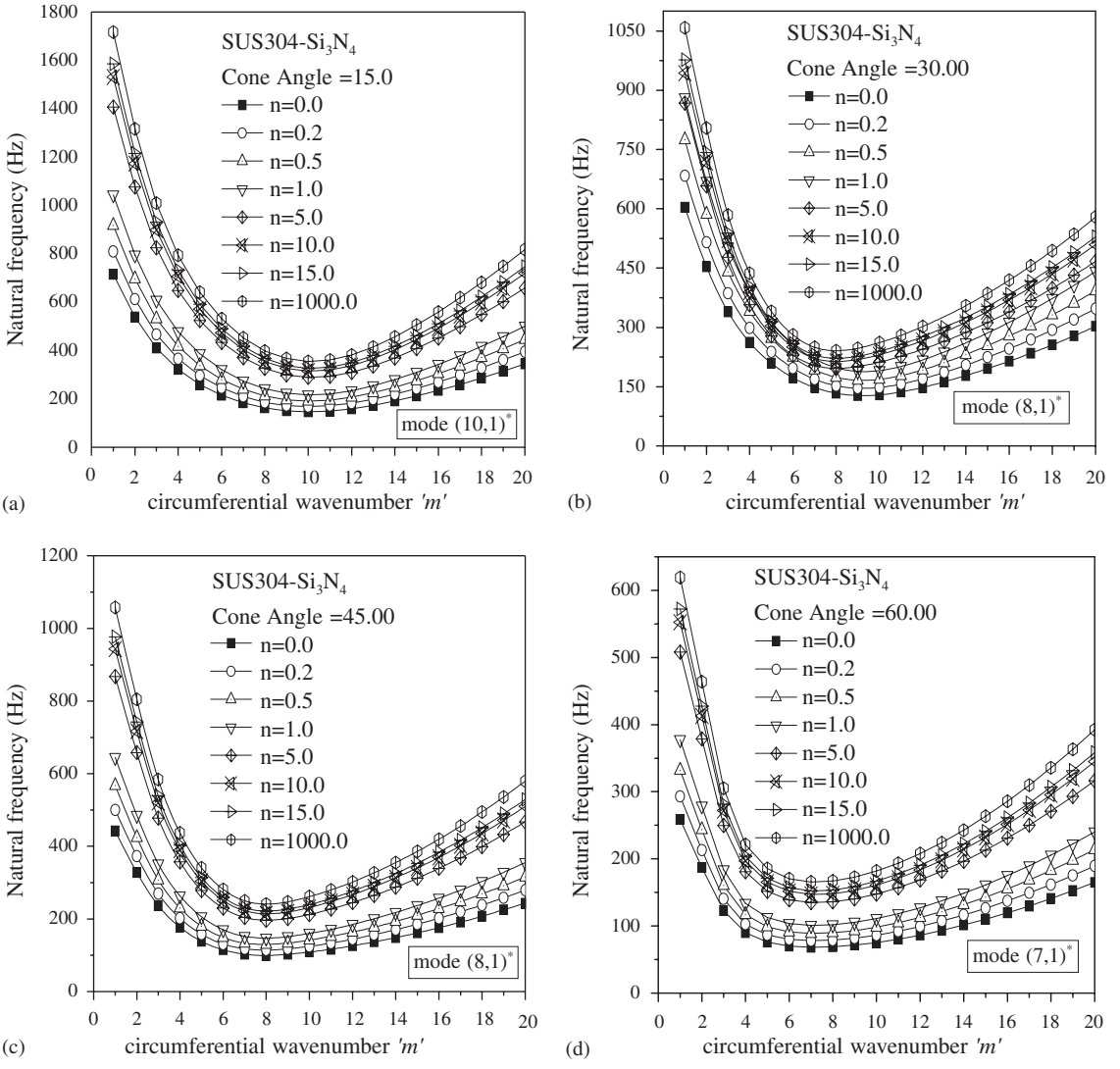

Fig. 5. (a–d) Free vibration frequency of SUS304-Si_3N_4 truncated FGM conical shell considering temperature distribution and thereby accounting for temperature-dependent material properties with different semi-vertex angle for chosen power law index, $l/r = 1.0438$, $r/h = 292.0$.

FGM shell stiffness matrix and along with mass matrix, a system of second-order linear differential equations are solved for free vibration frequencies for various circumferential modes. The results are illustrated in Figs. 7–10.

It is clear from Fig. 7 that the natural frequencies decrease with an increase in temperature. From the free vibration studies, it is clear that the natural frequencies are higher for higher values of the power law index. Further, higher the power law index, higher is the buckling temperature; of course, this depends on the constituent materials used for FGM. Further, the characteristic variation of the natural frequency with respect to temperature depends on the mode numbers.

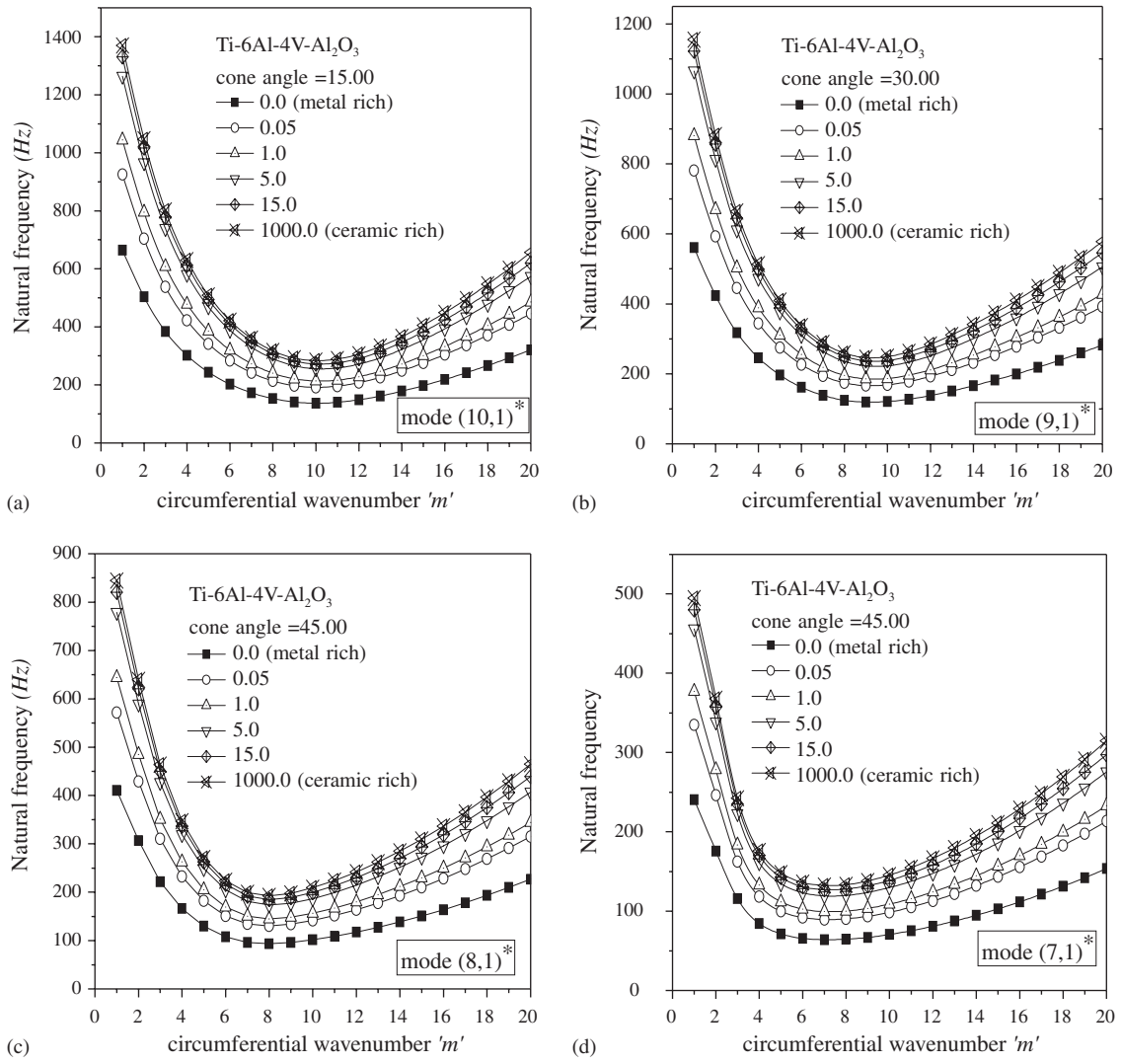

Fig. 6. (a–d) Free vibration frequency of SUS304-Si_3N_4 truncated FGM conical shell considering temperature distribution and thereby accounting for temperature-dependent material properties with different semi-vertex angles for chosen power law index, $l/r = 1.0438$, $r/h = 292.0$.

Referring to Figs. 7(a) and (f), for modes (1,1) and (18,1), respectively, it is seen that the fall in the natural frequency is not appreciable with an increase in temperature. This is probably due to the membrane effects dominating over the meridional stress resultants due to temperature rise for lower mode (1,1). For higher mode (18,1), the bending strain energy dominates the meridional stress resultants. However, the sudden and gradual decrease in the natural frequencies for higher temperature may be noted where probably the meridional stress resultants overtake the effect of bending strain energy. For the mode like (10,1), which corresponds to the lowest natural frequency of the shell, the membrane effect as well as the bending strain energy is minimal

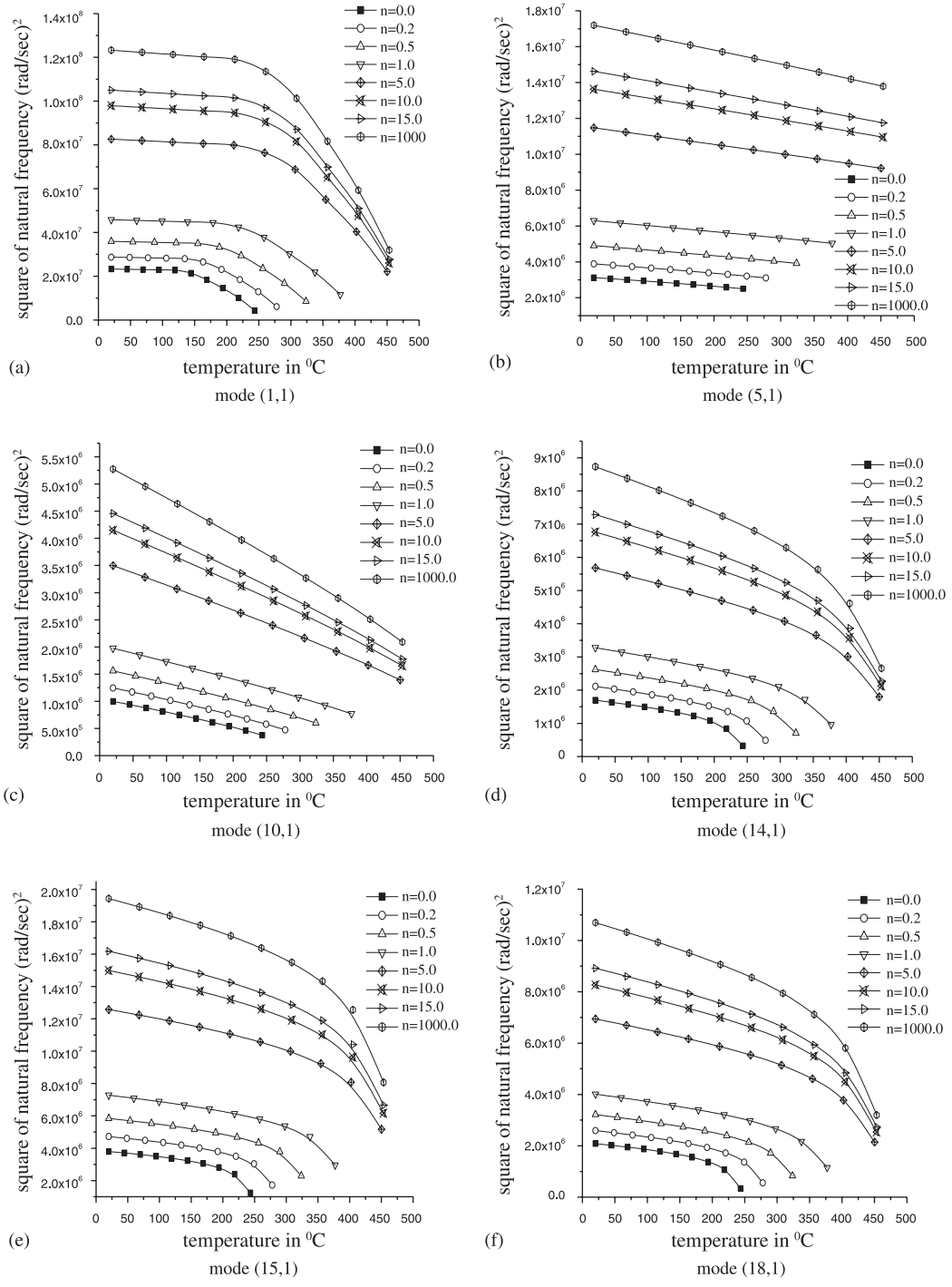

Fig. 7. (a–f) Effect of temperature on the free vibration frequencies of SUS304-Si_3N_4 truncated FGM conical shell having semi-vertex angle $\beta_{sv} = 15.0$. $l/r = 1.0438$, $r/h = 292$.

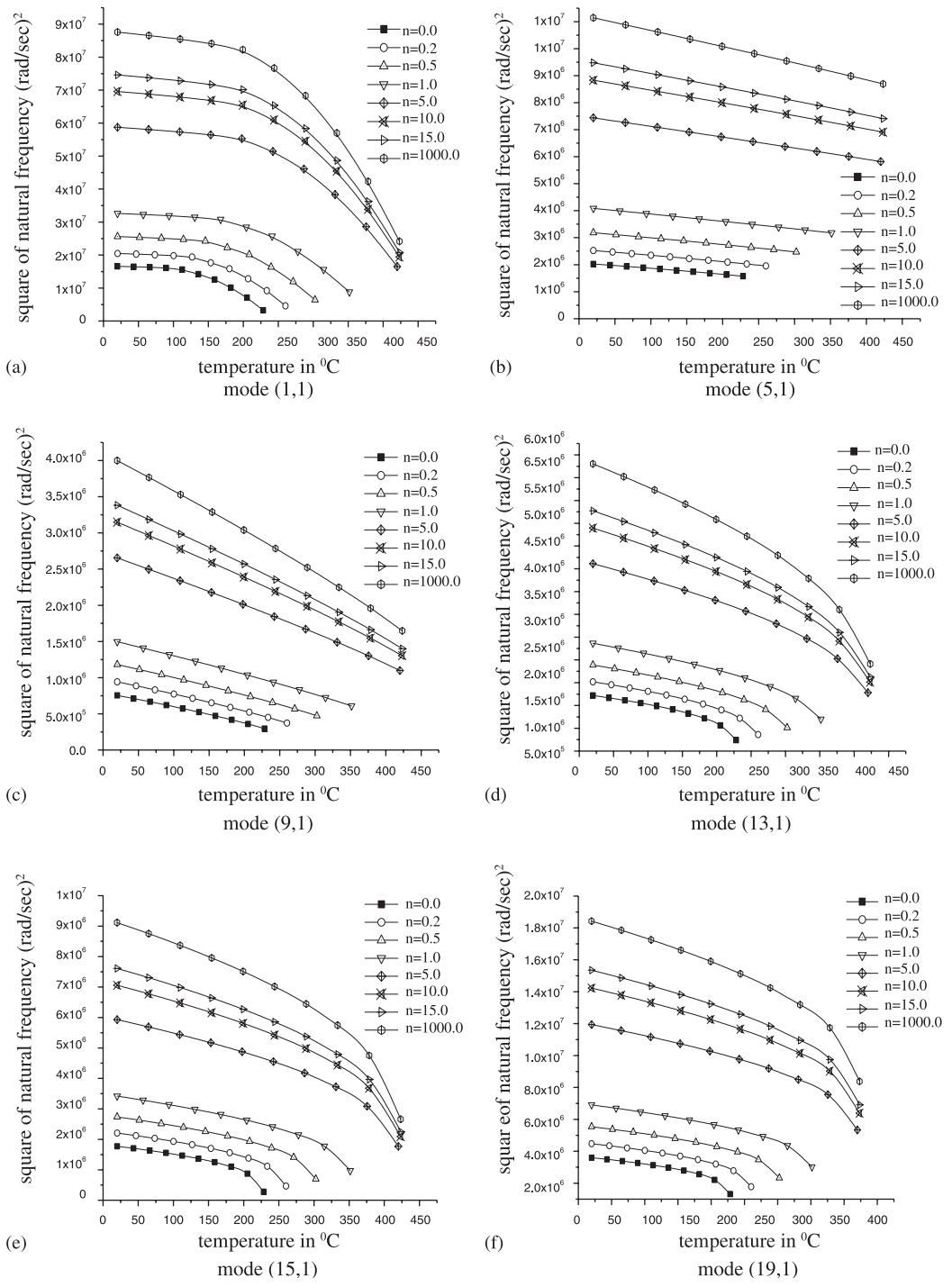

Fig. 8. (a–f) Effect of temperature on the free vibration frequencies of SUS304-Si_3N_4 truncated FGM conical shell having semi-vertex angle $\beta_{sv} = 30.0$. $l/r = 1.0438$, $r/h = 292$.

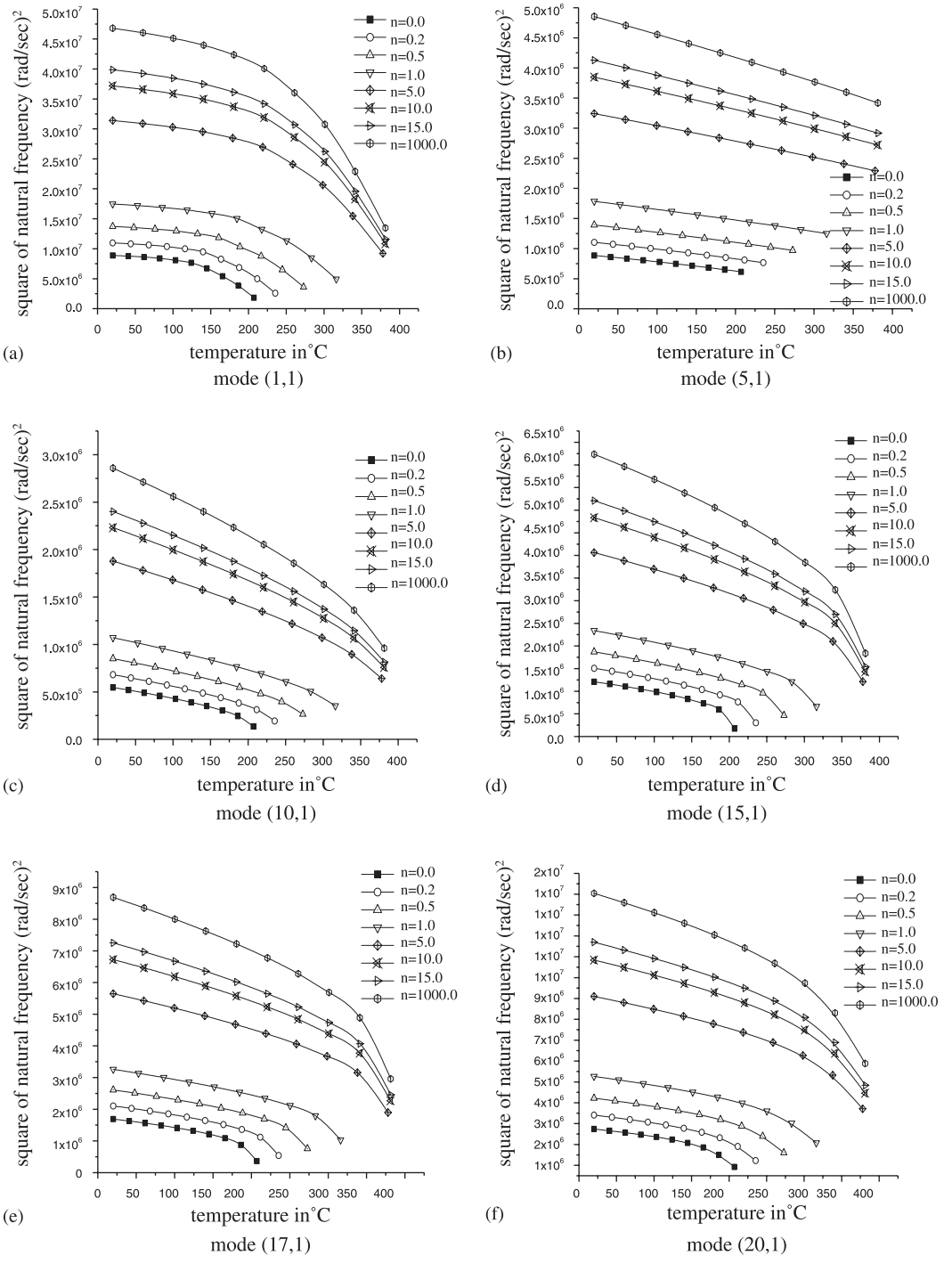

Fig. 9. (a–f) Effect of temperature on the free vibration frequencies of SUS304-Si_3N_4 truncated FGM conical shell having semi-vertex angle $\beta_{sv} = 45.0$. $l/r = 1.0438$, $r/h = 292$.

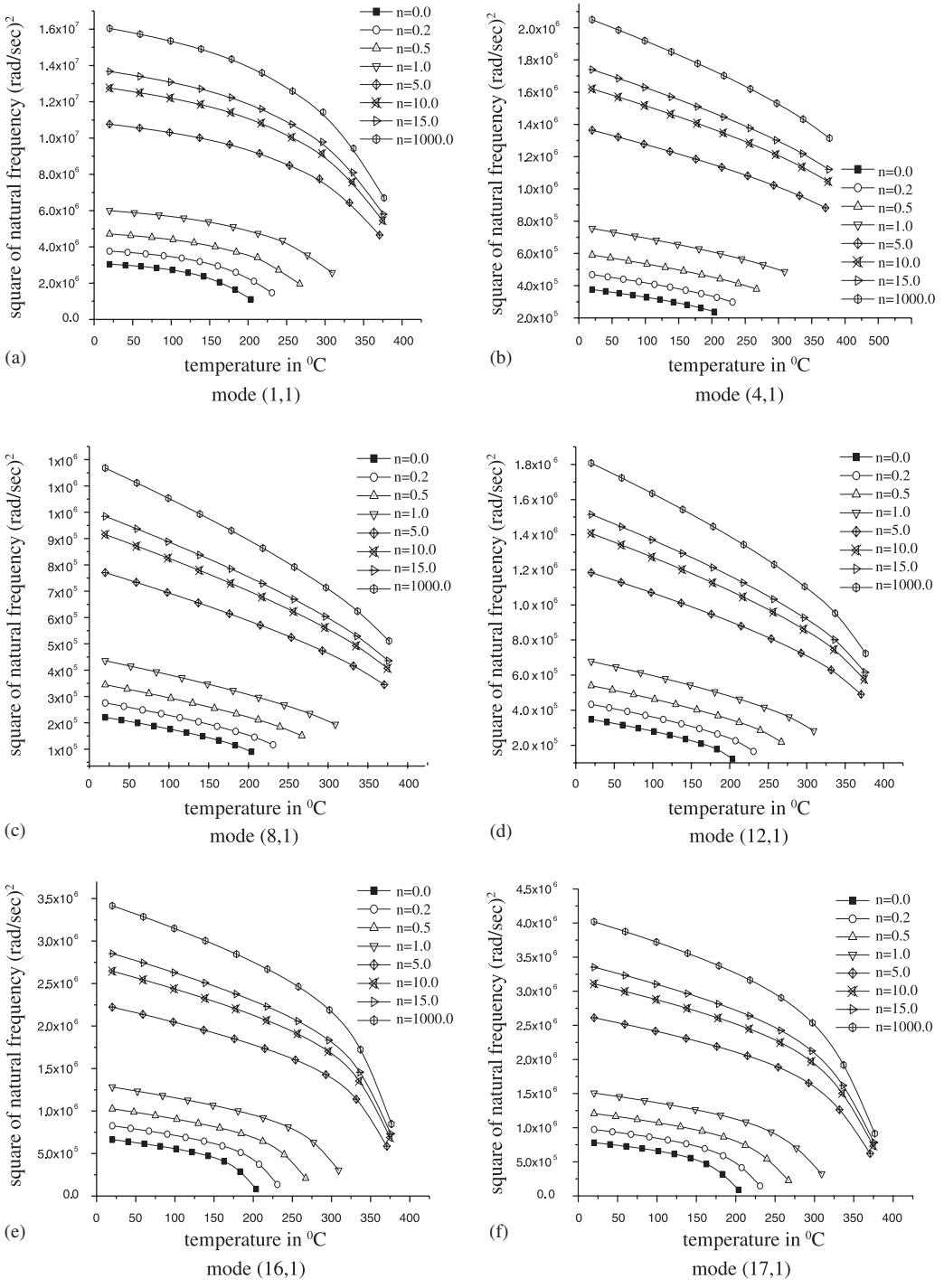

Fig. 10. (a–f) Effect of temperature on the free vibration frequencies of SUS304-Si_3N_4 truncated FGM conical shell having semi-vertex angle $\beta_{sv} = 60.0$. $l/r = 1.0438$, $r/h = 292$.

(Fig. 7(c)). Hence, the fall in frequency is smooth and gradual as the temperature increases, and for temperature close to the buckling temperature, the frequencies take on very low values. Now mode (15,1) is considered; it is the mode corresponding to the lowest thermal buckling temperature. Hence, the meridional stress resultants are large and compressive in nature for a given rise in temperature. Also, mode (15,1) is associated with reasonably high bending strain energy. But the high meridional stress resultants dominate the bending strain energy and cause the fall in natural frequencies gradually and continuously as the temperature increases (Fig. 7(d)), similar to that observed for the case of mode (10,1). However, the magnitudes of the frequency are slightly higher compared to mode (10,1). Thus, it is clear that the effect of temperature is felt more for the modes corresponding to the lowest natural frequency and lowest thermal buckling temperature and more so for the lowest natural frequency mode. Similar results were obtained for FGM truncated conical shell having different semi-vertex angles. As we can see, as the semi-vertex angle of the cone increases, the critical buckling mode and lowest natural frequency mode change. However, typical results for the variation of natural frequencies for semi-vertex angle $= 30^\circ$ are illustrated in Figs. 8(a)–(f) and are now considered for discussion. Here results are presented for modes (9,1) and (13,1), which correspond to the lowest natural frequency of the shell. The smooth, gradual and continuous fall in the natural frequencies may be noted (Figs. 8(c) and (d)) as the temperature increases. The lowest buckling temperature mode is (15,1) and also another mode close to this is (13,1). For these modes the variation of the natural frequencies with respect to temperatures is presented in Figs. 8(e) and (f). For modes (15,1) and (19,1) the meridional stress resultants are high. Referring to Fig. 8(b), the modes (15,1) and (19,1) are on the higher side, where the bending strain energy dominates. Hence, for initial rise in temperature, the bending strain energy probably dominates the meridional stress resultants due to temperature rise. However, for higher temperatures and temperatures close to the buckling temperature, the magnitude of the meridional stress resultants overtakes bending strain energy and causes the frequencies to fall drastically (Figs. 8(d) and (e)). A similar discussion holds good for semi-vertex angles 45° and 60° illustrated in Figs. 9(a) and (e) and Figs. 10(a) and (e).

9. Conclusion

A linear thermoelastic thermal buckling analysis of functionally graded truncated conical shells with different semi-vertex angles based on the semi-analytical finite element method has been presented. The FGM conical shell is graded in the thickness direction and a simple power law index governs the metal–ceramic constituents profile across the thickness. The converged temperature distribution becomes the thermal loading on the shell with the thermal buckling temperature being evaluated until convergence is obtained. The following conclusions are arrived at from the investigation.

1. The magnitude of the lowest buckling temperature greatly depends on the composition of the metal–ceramic constituent. The thermal buckling temperature depends on the power law index. Materials with lower coefficient of thermal expansion will have high thermal buckling temperature.
2. With an increase in the semi-vertex angle of the FGM truncated conical shell, the critical thermal buckling temperature reduces.

3. The critical buckling temperature decreases with increase in the ratios of r/h, as expected.
4. Thermal buckling strength is reduced when the temperature-dependent properties are taken into consideration.
5. The critical buckling temperature for the FGM conical shell obtained by linear temperature gradient across the thickness is not necessary to be twice that of the shells under uniform temperature rise, but lower than $2T_{\text{critical}}$. This may be because the above study incorporates the temperature-dependent material property.
6. The lowest critical buckling temperature mode decreases first with an increase in semi-vertex angle then again increases for angle 60° for same r/h ratios.
7. The free vibration natural frequencies of FGM conical shells are typically characterized by the bathtub curve, when the axial mode frequencies are plotted for various circumferential harmonics. In addition, it is found that an increase in semi-vertex angle brings down the natural frequency.
8. The effect of temperature on the natural frequency of FGM shell is to reduce the natural frequency with an increase in temperature as expected.
9. The effect of temperature on the natural frequency is more for the modes with the lowest natural frequency and for modes with the lowest critical buckling temperature.
10. It is important to check the strength of FGM for thermal buckling while considering design aspects by taking into account temperature-dependent material properties.

References

[1] M. Koizumi, FGM activities in Japan, *Composites, Part B* 28 (1997) 1–4.
[2] M. Koizumi, N. Niino, Overview of FGM research activities in Japan, *Material Research Society Bulletin* 20 (1995) 19–21.
[3] K. Ichikawa, *Functionally graded materials in the 21st century, A Workshop on Trends and Forecasts*, Kluwer Academic Publisher, Boston, 2001.
[4] S. Suresh, A. Mortensen, *Fundamentals of Functionally Graded Materials*, IOM communications, London, 1998.
[5] B.V. Sankar, J.T. Tzeng, Thermal stress in functionally graded beams, *AIAA Journal* 40 (6) (2002) 1228–1232.
[6] S.Y. Lu, L.K. Chang, Thermal buckling of conical shells, *AIAA Journal* 5 (1967) 1877–1882.
[7] S.Y. Lu, L.K. Chang, Nonlinear thermal buckling of conical shells, *International Journal of Mechanical Science* 34 (1967) 93–111.
[8] P.C. Dumir, G.P. Dube, A. Mullick, Axisymmetric static and dynamic buckling of laminated thick truncated conical cap, *International Journal of Non-Linear Mechanics* 37 (2003) 903–910.
[9] M. Stern, Analysis of thermal stresses in conical shells, *Journal of Aeronautical Sciences* 22 (1955) 506–508.
[10] J.H. Huth, Thermal stresses in conical shells, *Journal of Aeronautical Sciences* 20 (1953) 613–616.
[11] D. Bushnell, S. Smith, Stress and buckling of nonuniformly heated cylindrical and conical shells, *AIAA Journal* 9 (1971) 2314–2321.
[12] J. Tani, Influence of axisymmetric initial deflections on the thermal buckling of truncated conical shells, *Nuclear Engineering and Design* 48 (1978) 393–403.
[13] A.A. Lakis, P. Vandyke, H. Ouriche, Dynamic analysis of anisotropic fluid-filled conical shells, *Journal of Fluids and Structures* 6 (1992) 135–162.
[14] P. Jianping, I.E. Harik, Axisymmetric pressure and thermal gradients in conical missile tips, *Journal of Aerospace Engineering* 4 (1991) 237–255.
[15] C.P. Wu, S.J. Chiu, Thermally induced dynamic instability of laminated composite conical shells, *International Journal of Solids Structures* 39 (2002) 3001–3021.

[16] J.N. Reddy, C.D. Chin, Thermomechanical analysis of functionally graded cylinders and plates, *Journal of Thermal Stresses* 21 (1998) 593–626.
[17] K.M. Liew, S. Kitipornchai, X.Z. Zhang, C.W. Lim, Analysis of the thermal stress behavior of functionally graded hollow circular cylinders, *International Journal of Solids and Structures* 40 (2003) 2355–2380.
[18] T. Tauchert, Thermal buckling of plates and shells, *Applied Mechanics Reviews* 46 (1993) 485–506.
[19] G.N. Praveen, C.D. Chin, J.N. Reddy, Thermoelastic analysis of functionally graded ceramic-metal cylinder, *Journal of Engineering Mechanics* 125 (1999) 1259–1267.
[20] A.H. Sofiyev, The stability of functionally graded truncated conical shells subjected to aperiodic impulsive loading, *International Journal of Solids Structures* 41 (2004) 3411–3424.
[21] R.K. Bhangale, Thermal buckling of functionally graded beam, *Proceedings of the Third International Conference on Theoretical Applied and Computational Mechanics IIT Kharagpur* (2004) 274–277 (27–30 December).
[22] R. Javaheri, M.R. Eslami, Thermal buckling of functionally graded plates based on higher order theory, *Journal of Thermal Stresses* 25 (2002) 603–625.
[23] R.K. Bhangale, N. Ganesan, P. Chandramouli, Free vibration and buckling analysis of functionally graded cylindrical shell conveying hot liquid sodium, *Proceeding of the First International Congress on Computational Mechanics and Simulations IIT Kanpur* (2004) 604–611 (9–12 Decemeber).
[24] R. Kadoli, *Studies on shells of revolution in thermal environment*, Ph.D. Thesis, IIT Madras, 2003.
[25] R.K. Bhangale, N. Ganesan, A linear theromoelastic buckling behaviour of functionally graded hemispherical shells with cut-out at apex, *International Journal of Structural Stability and Dynamics* 5 (2005) 185–215.
[26] R. Kadoli, N. Ganesan, A theoretical analysis of linear thermoelastic buckling of composite hemispherical shells with cut-out at apex, *Composite Structure* 68 (2004) 87–101.
[27] L. Banks Sills, R. Eliasi, Y. Berlin, Modeling of functionally graded materials in dynamic analyses, *Composites: Part B Engineering* 33 (2002) 7–15.
[28] Y. Tanigawa, Some basic thermoelastic problems for nonhomogeneous structural materials, *Applied Mechanics Review* 48 (1995) 287–300.
[29] O.C. Zienkiewicz, R.L. Taylor, fourth ed., *The Finite Element Method, vol. 2, Solids and Fluid Mechanics, Dynamics and Non-Linearity*, McGraw-Hill Book Company, Singapore, 1991.
[30] C.T.F. Ross, *Pressure Vessels under External Pressure: Static and Dynamics*, Elsevier Applied Science, London, 1990.
[31] R.D. Cook, D.S. Malkus, M.E. Plesha, *Concepts and Applications of Finite Element Analysis*, third ed., Wiley, Singapore, 2000.
[32] J.N. Reddy, *An Introduction to the Finite Element Method*, McGraw-Hill International Editions, Singapore, 1984.